JGR Solid Earth

RESEARCH ARTICLE
10.1029/2020JB020068

Remagnetization of Red Beds on the Tibetan Plateau: Mechanism and Diagnosis

Wentao Huang[1,2], Michael J. Jackson[3], Mark J. Dekkers[4], Peat Solheid[3], Yang Zhang[5], Shihu Li[6], Zhaojie Guo[7], and Lin Ding[1]

[1]Key Laboratory of Continental Collision and Plateau Uplift, Institute of Tibetan Plateau Research, and Center for Excellence in Tibetan Plateau Earth Sciences, Chinese Academy of Sciences, Beijing, China, [2]Department of Earth and Environmental Sciences, University of Rochester, Rochester, NY, USA, [3]Institute for Rock Magnetism, Department of Earth Sciences, University of Minnesota, Minneapolis, MN, USA, [4]Department of Earth Sciences, Utrecht University, Utrecht, Netherlands, [5]The First Monitoring and Application Center, China Earthquake Administration, Tianjin, China, [6]Lancaster Environment Centre, Lancaster University, Lancaster, UK, [7]Key Laboratory of Orogenic Belts and Crustal Evolution, Ministry of Education, School of Earth and Space Sciences, Peking University, Beijing, China

Key Points:
- Remagnetized red beds contain large amounts of fine-grained authigenic hematite and goethite
- Diagenetic alteration induced by heating and/or fluid circulation is probably the main reason for the remagnetization in red beds
- Thermomagnetic behavior and appearance of goethite are two reliable criteria for diagnosing remagnetization in red beds

Supporting Information:
- Supporting Information S1

Correspondence to:
W. Huang,
whuang28@ur.rochester.edu

Citation:
Huang, W., Jackson, M. J., Dekkers, M. J., Solheid, P., Zhang, Y., Li, S., et al. (2020). Remagnetization of red beds on the Tibetan Plateau: Mechanism and diagnosis. *Journal of Geophysical Research: Solid Earth*, *125*, e2020JB020068. https://doi.org/10.1029/2020JB020068

Received 30 APR 2020
Accepted 26 JUN 2020
Accepted article online 11 JUL 2020

Abstract Red beds are important targets for paleomagnetic studies, yet discriminating secondary chemical remanent magnetization (CRM) from primary depositional remanent magnetization (DRM) in them remains challenging. Here we reanalyze the thermal demagnetization data of and conduct comprehensive rock magnetic, Mössbauer spectroscopic and petrographic studies on red beds from four Cenozoic basins on the eastern Tibetan Plateau (China): the Gongjue, Nangqian, Shanglaxiu, and Jinggu basins. The red beds in the latter two basins are remagnetized, as are most Nangqian red beds. The Gongjue red beds and some Nangqian red beds retain a DRM. Our results reveal that detrital (titano)magnetite and hematite are well preserved in red beds retaining the DRM, whereas remagnetized red beds contain large amounts of authigenic hematite and goethite with detrital Fe-bearing minerals strongly altered. Postdepositional diagenetic alteration induced by heating and/or fluid circulation related to magmatism and/or crustal deformation is probably the main reason for the remagnetization. Hematite carrying the CRM in remagnetized red beds has wide distribution of grain size and unblocking temperature spectra, while hematite carrying the DRM is usually coarse and has confined unblocking temperature spectrum. This can be used as a criterion for diagnosing remagnetization. Nanoscale goethite appears to occur only in remagnetized red beds: another sensitive criterion for discriminating CRM from DRM. These property-based criteria constrain the origin of the NRM in red beds better than the classic paleomagnetic field tests. Our research emphasizes that integrated rock magnetic, Mössbauer spectroscopic and petrographic studies provide robust tools to diagnose remagnetization in red beds.

1. Introduction

Red beds, siliciclastic rocks pigmented by hematite, can record geologically stable natural remanent magnetizations (NRMs) and thus are an important archive of global paleomagnetic data for investigating geomagnetic field behavior, paleogeography, and geochronology (e.g., Bosboom et al., 2014; Kruiver et al., 2000; Xian et al., 2019). A long-standing debate known as "the red bed controversy" exists, however, concerning the timing of NRM acquisition in red beds relative to their deposition age (Tauxe et al., 1980; van der Voo & Torsvik, 2012). On the one side, it has been documented that detrital hematite can carry a primary depositional remanent magnetization (DRM) dating back to the depositional age of the red beds. On the other side, chemical remanent magnetization (CRM) carried by authigenic hematite growing in situ after deposition is omnipresent and can partially to completely replace the DRM, thus remagnetizing red beds. Paleomagnetic studies of red beds on the Tibetan Plateau (Figure 1a) have often yielded controversial geologic interpretations. For example, the Cretaceous paleolatitudes of the Qiangtang terrane constrained from red beds are 30–36°N (reference location of 29°N, 100°E; same for below) (Huang et al., 1992; Otofuji et al., 1990), much higher than the robust results of the Lhasa terrane of ~20°N (Huang et al., 2015; Lippert et al., 2014; Ma et al., 2014). If these results from red beds were correct, the Qiangtang terrane would have been separated from the Lhasa terrane by more than 1,000 km, which is inconsistent with the geologic observations that the Lhasa terrane welded to the south of the Qiangtang terrane in the Late Jurassic (e.g., Ma et al., 2017).

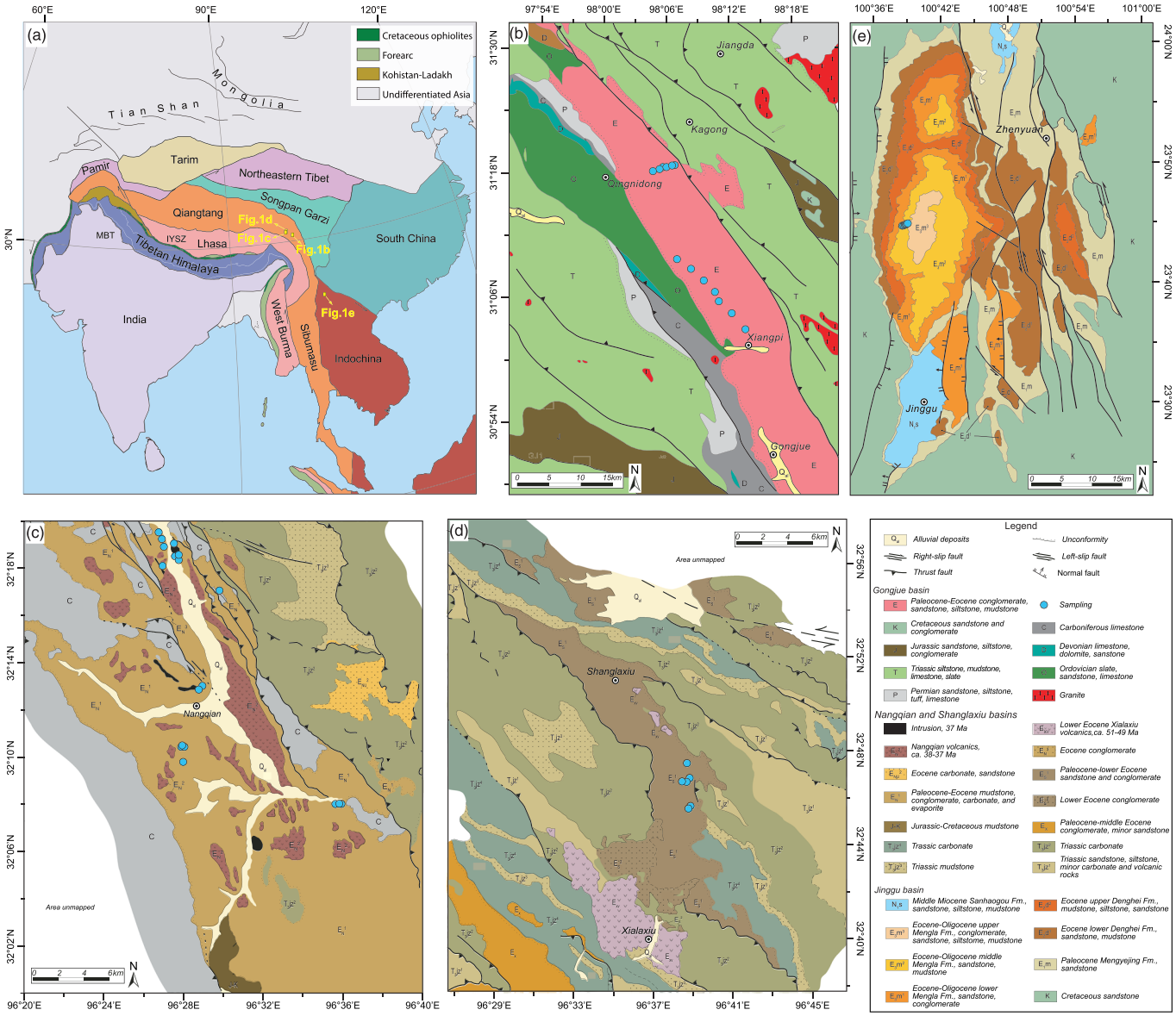

Figure 1. (a) Map with the tectonic units of the India-Asia collision zone. (b–e) Simplified geologic maps of the Gongjue, Nangqian, Shanglaxiu, and Jinggu basins (Li et al., 2017; Spurlin et al., 2005; Zhang et al., 2018) with paleomagnetic sampling localities of red beds plotted as filled blue dots.

Therefore, we must check the possibility of remagnetization in these red beds, and in red beds elsewhere when yielding suspicious results from a general geological framework.

Traditional paleomagnetic field tests are not always available to constrain the origin of NRM in red beds. Even when available, they often fail to reveal remagnetization occurring before folding but long after deposition, which leads to a false-positive fold test (e.g., Li et al., 2017), and remagnetization occurring in a long geologic intervals of dual magnetic polarities, which leads to a false-positive reversals test (e.g., Huang & Opdyke, 2015). Therefore, efforts have been made to search for criteria to diagnose remagnetization in red beds, independent from paleomagnetic directions. Liu et al. (2011) found that remagnetized red beds have widely distributed S ratios (defined as –IRM-0.3T/IRM1.8T), whereas S ratios of red beds retaining DRM are <0.15. For detecting remagnetization in red beds, this criterion is ambiguous and leaves a fairly large uncertainty. Another criterion comes from experimental studies, which show that hematite carrying CRM is fine grained and has widely distributed unblocking temperature spectra from 200°C to 600°C, while

hematite carrying DRM is usually coarser grained and has a more confined unblocking spectrum from ~600°C to 680°C. The concave and convex shape of the thermal decay curves is thus proposed to indicate CRM and DRM, respectively (Jiang et al., 2015). Uncertainty still exists, however, in the use of this criterion because paleomagnetic studies on natural samples reveal that the unblocking temperature spectra of the CRM can overlap with those of the DRM and extend up to the Néel temperature of hematite (Jiang et al., 2017; Swanson-Hysell et al., 2019). In a recent study of the Paleogene red beds in the Nangqian Basin (eastern Tibetan Plateau), we have identified that remagnetized red beds contain large amounts of nanogoethite, whereas goethite is not present in red beds retaining the DRM (Huang, Jackson, Dekkers, Solheid, et al., 2019). The presence of abundant nanoscaled goethite seems like a sensitive criterion for diagnosing remagnetization in red beds.

Here we further test whether differences in unblocking temperature spectra and the presence of goethite are universal property-based criteria for diagnosing remagnetization to better understand DRM preservation and CRM acquisition mechanisms in red beds. We evaluate results from red beds in Cenozoic basins (Gongjue Basin, Shanglaxiu Basin, and Jinggu Basin) on the eastern Tibetan Plateau (Figure 1). The Gongjue red beds record a DRM (Li et al., 2020; Tong et al., 2017; Zhang et al., 2018), and red beds in the Shanglaxiu and Jinggu basins are remagnetized (Li et al., 2017; Roperch et al., 2017). The situation in the Nangqian Basin is more complicated: most red beds in the Nangqian Basin are remagnetized, but some retain a DRM (Huang, Jackson, Dekkers, Solheid, et al., 2019). Specifically, we analyze the thermal demagnetization behaviors of the NRM in all of these red beds, apply comprehensive rock magnetic experiments, conduct Mössbauer spectroscopy analysis, and carry out scanning electron microscopy (SEM) examinations with associated energy-dispersive X-ray spectrometry (EDS) analysis. We use these observations to compare the magnetic mineralogy and grain size, and diagenetic conditions of remagnetized red beds to those of the red beds retaining the DRM. We discuss the acquisition mechanisms of the primary and secondary NRMs in red beds. Finally, we propose property-based criteria for diagnosing remagnetization in red beds, which can be easily applied to red beds deposited elsewhere during other geologic periods.

2. Geological Background, Previous Paleomagnetic Investigations, and Sampling

The Cenozoic Gongjue, Nangqian, and Shanglaxiu basins are located in the eastern Qiangtang terrane (Figure 1), which amalgamated to the northeastern Tibetan Plateau in the Late Triassic (e.g., Song et al., 2015). The formation of these basins was controlled by a series of small thrusts related to contractional deformation during the initial stage of the India-Asia collision (Horton et al., 2002; Studnicki-Gizbert et al., 2008). The Gongjue Basin is mainly filled with red beds (sandstone, siltstone, and conglomerate) and evaporites (carbonate, gypsum, and salt). Recent magnetostratigraphic study, together with palynological assemblages and isotopic dates, constrains deposition of these red beds at 69–41.5 Ma (Li et al., 2020, and references therein). The Nangqian Basin fill is dominated by reddish mudstone and siltstone, interbedded with minor limestone and gypsum (Li et al., 2018). The occurrence of Paleogene fossils and isotopic dating of the detrital zircons in red beds, intrusions, and volcanic rocks interbedded with the uppermost strata constrain the depositional age at >38 Ma (Horton et al., 2002; Spurlin et al., 2005; Zhang et al., 2019). The Shanglaxiu Basin contains thick red sandstone interbedded with muddy limestone, gypsum, and a few volcanic layers. The Cenozoic infill of this basin is older than ~50 Ma because an unconformity exists between the overlying Eocene volcanic rocks and the uppermost basin (Horton et al., 2002).

The Jinggu Basin is located in the north of the Indochina block (Figure 1). Formation of the basin was controlled by a left-lateral strike-slip fault, and the basin fill is dominated by Cretaceous to Miocene red sandstone, siltstone, and mudstone, preserved in a N-S trending syncline (BGMRYP, 1990).

Positive fold and reversal tests support a primary origin of the NRM recorded by the Gongjue red beds (Li et al., 2020; Tong et al., 2017; Zhang et al., 2018). In contrast, paleomagnetic results of the Jinggu red beds are of exclusive normal polarity, although they pass the fold test (Li et al., 2017). Paleomagnetic results of the Shanglaxiu red beds are distinct from robust results of the interbedded volcanic rocks in both declination and inclination (Cogné et al., 1999; Roperch et al., 2017). Those Paleogene red beds in the Jinggu and Shanglaxiu basins are thus argued to be remagnetized by those authors. Red beds in the Nangqian Basin variably record overprints related to nearby magmatism. The DRM in most samples has been replaced or

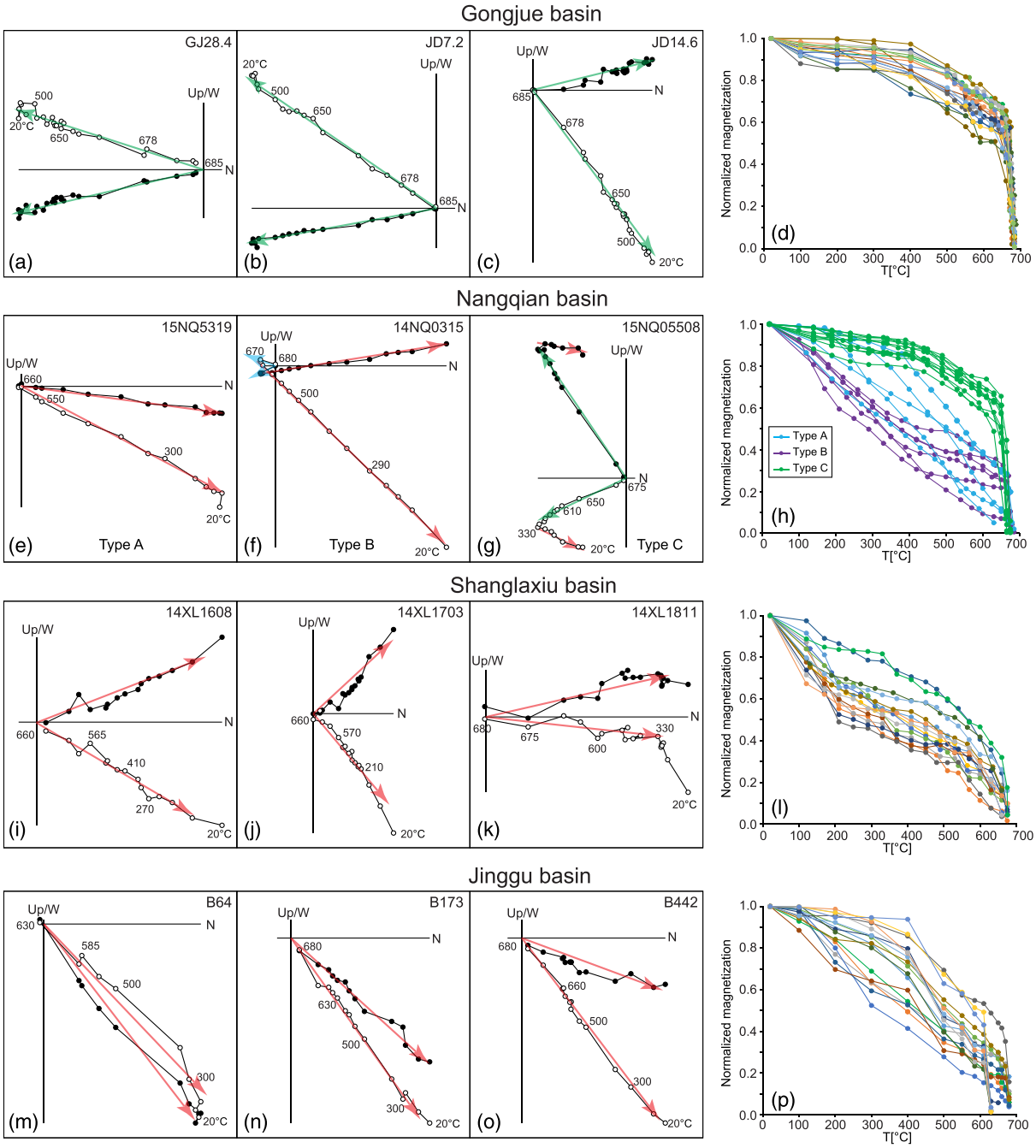

Figure 2. Thermal demagnetization trajectories of representative samples in geographic coordinates and corresponding normalized thermal decay curves (summed vector differences) of the red bed samples from the Gongjue, Nangqian, Shanglaxiu, and Jinggu basins. In the Zijderveld diagrams, closed symbols are projections on the horizontal plane and open symbols on the vertical plane. Gongjue samples are nonremagnetized; samples from the Shanglaxiu and Jinggu basins are remagnetized; Types A and B samples from the Nangqian Basin are remagnetized, whereas Type C samples from the Nangqian Basin retain a primary NRM (Huang, Jackson, Dekkers, Solheid, et al., 2019). Green arrows show fitted directions of the NRM with primary origin; red arrows are fitted NRM directions from remagnetized samples; blue arrow in (f) is the fitted direction of remanence isolated above 650°C from Type B samples in the Nangqian Basin; this remanence has been biased by the overprint (Huang, Jackson, Dekkers, Solheid, et al., 2019).

contaminated by a CRM, but a small portion of the samples retain a DRM (Huang, Jackson, Dekkers, Solheid, et al., 2019). In the present research, we focus on red bed samples from the Gongjue Basin studied by Zhang et al. (2018), the Nangqian and Shanglaxiu basins studied by Roperch et al. (2017), and the Jinggu Basin studied by Li et al. (2017).

3. Thermal Demagnetization Behaviors of the NRMs

Thermal demagnetization results of red beds from the Gongjue, Nangqian, Shanglaxiu, and Jinggu basins are from previous studies (Li et al., 2017; Roperch et al., 2017; Zhang et al., 2018). For the red bed samples from the Gongjue Basin, a stable intermediate high temperature component decaying linearly to the origin up to 685°C was isolated after removing a random viscous component at low temperature (<300°C) (Figures 2a–2c). This component is of dual polarities and passes both fold and reversal tests (Tong et al., 2017; Zhang et al., 2018). The thermal decay curves of the NRM in these red beds are convex and feather a small break in slope at ~580°C and a marked and sharp decay between 650°C and 685°C (Figure 2d).

Three types of demagnetization behavior were observed in red beds samples from the Nangqian Basin: Type A samples show a single component of normal polarity up to 680°C (Figure 2e); Type B samples have a low-intermediate temperature component of normal polarity isolated below 650°C, followed by a very weak high-temperature component of reversed polarity isolated above 650°C (Figure 2f); and Type C samples record an intermediate high temperature component of reversed polarity isolated from 300–600°C to 680°C after removing a low-intermediate temperature of normal polarity (Figure 2g). The normal polarity component from the Nangqian red beds is an overprint, which is indistinguishable in direction from the primary NRM of the igneous rocks in the basin (Roperch et al., 2017). The common true mean direction test between the overprint in red beds and primary NRM in igneous rocks is Class C. The high-temperature component of Type B samples is also contaminated by the overprint; only the intermediate high temperature component of Type C samples represents a primary NRM (Huang, Jackson, Dekkers, Solheid, et al., 2019). The convex thermal decay curves of Type C samples are similar to those of the Gongjue red beds, whereas Type A samples have linear-convex thermal decay curves, and Type B samples are characterized by concave thermal decay curves with a sharp decrease in magnetization above 650°C (Figure 2h). Another notable distinction between Types A and B and Type C samples is that Types A and B samples have quickly lost the majority (>70%) of their NRM up to 650°C, whereas Type C samples retain >50% of their NRM up to 650°C (Figure 2h).

Red beds from the Shanglaxiu and Jinggu basins record NRM of exclusively normal polarity (Figures 2i–2k and 2m–2o). The intermediate high temperature component, isolated between ~300°C and 680°C, represents a secondary NRM (Li et al., 2017; Roperch et al., 2017). A magnetite contribution, if any, is marginal at best. Thermal decay curves of the NRM for these samples are linear convex (Figures 2l and 2p), similar to those of the remagnetized Types A and B sample in the Nangqian Basin. Most samples have lost >70% of their NRM up to 650°C.

4. Rock Magnetism

To identify magnetic carries and their grain size distributions in these red beds, we applied a series of rock magnetic experiments. Details on measurement procedures and data analysis protocols are provided in the supporting information.

4.1. High-Temperature Magnetic Susceptibility

Multicycle high-temperature magnetic susceptibility versus temperature (χ-T) curves were acquired from 24 whole-rock samples (four samples from the Gongjue Basin, four from the Nangqian Basin, seven samples from the Shanglaxiu Basin, and nine from the Jinggu Basin). χ-T curves of samples from the Gongjue Basin show a gradual and reversible decrease in the magnetic susceptibility with two steep slope segments recognized at 540–580°C and 630–680°C (Figures 3a–3d), which are indicative of magnetite and hematite, respectively (Dunlop & Ödemir, 1997). For samples from the Nangqian Basin, χ-T curves of those retaining DRM are characterized by a quick decrease of the magnetic susceptibility below ~400°C, a hump between 400°C and 620°C, and a sharp drop at >620°C (Figures 3e and 3f). In contrast, remagnetized samples show quasi-linear yet reversible decrease in the magnetic susceptibility up to 570°C, followed by a small hump and then a sharp drop at >620°C (Figures 3g and 3h). Another difference is that samples retaining DRM keep a majority (>50%) of their magnetic susceptibility at 600°C, whereas remagnetized samples have lost most (>70%) of their magnetic susceptibility at 600°C (Figures 3e–3h). The χ-T curves of samples from the Shanglaxiu Basin are characterized by two quasi-linear and reversible descending trends of the susceptibility with an inflection point at ~500°C (Figures 3i–3l). The χ-T curves of samples from the Jinggu Basin are

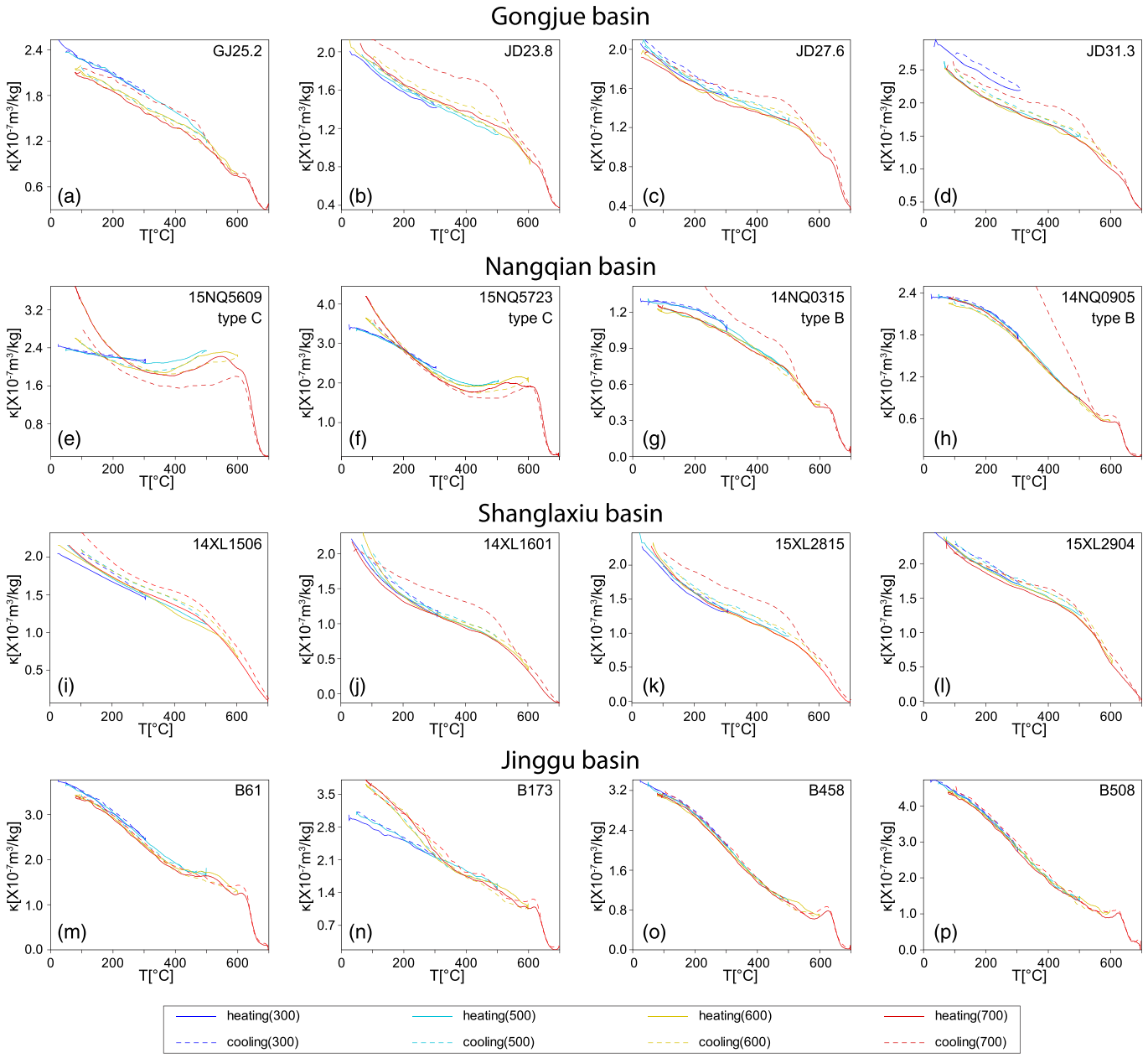

Figure 3. High-temperature susceptibility versus temperature (χ-T) curves of representative red beds samples from the Gongjue (a–d), Nangqian (e–h), Shanglaxiu (i–l), and Jinggu (m–p) basins.

similar to those of the remagnetized samples from the Nangqian Basin. Quasi-linear and reversible decrease in the magnetic susceptibility up to 570°C is followed by a small hump and then sharp drop at >620°C (Figures 3m–3p).

4.2. Room-Temperature Hysteresis Measurements

To supplement our previous measurements on 23 samples from the Gongjue Basin and 35 samples from the Nangqian Basin presented in Zhang et al. (2018) and Huang, Jackson, Dekkers, Solheid, et al. (2019), an additional 40 samples (4 from the Nangqian Basin, 15 from the Shanglaxiu Basin, and 21 from the Jinggu Basin) were processed for hysteresis measurements and isothermal remanent magnetization (IRM) acquisition. We realize that hematite is not magnetically saturated in the maximum available field of 1.4 Tesla. The coercive force (B_c) and remanent coercivity (B_{cr}) values are thus probably underestimated. Hysteresis loops of samples

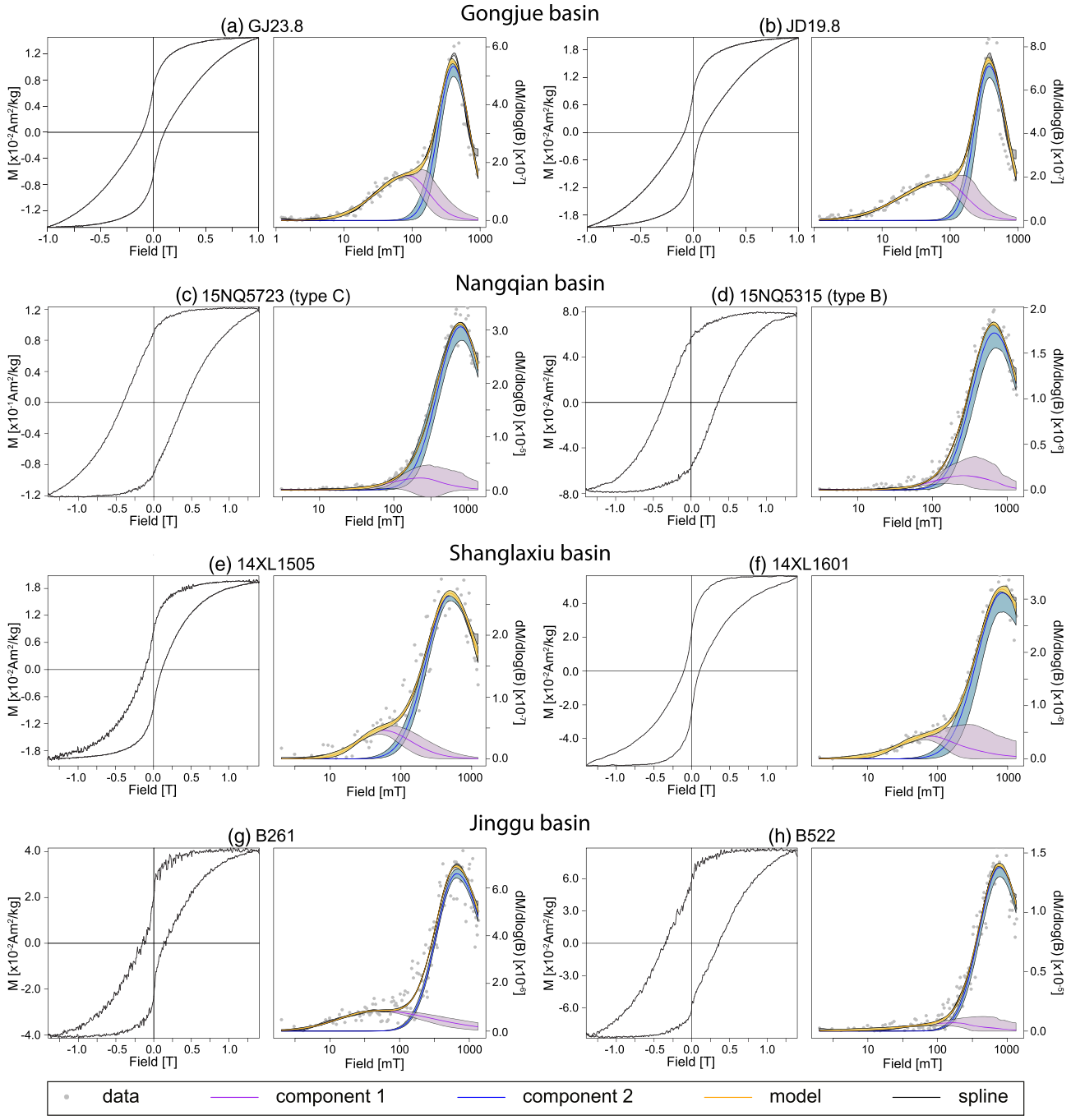

Figure 4. Room temperature hysteresis loops and component analysis of the isothermal remanent magnetization of representative red beds samples from the Gongjue (a, b), Nangqian (c, d), Shanglaxiu (e, f), and Jinggu (g, h) basins. Shaded area represents error envelopes of 95% confidence intervals.

from the Gongjue Basin are "wasp waisted" (Figures 4a and 4b), indicating the presence of magnetic mineral(s) with contrasting coercivities or grain sizes (Tauxe et al., 1996). The B_c and B_{cr} values for these samples vary from 26 to 238 mT and from 75 to 268 mT, respectively (Table S1). Together with the results from the χ-T curves (Figures 3a–3d), these observations suggest that the dominant magnetic carriers in the Gongjue red beds are magnetite and hematite. Indeed, two statistically significant components (Figures 4a and 4b) are used to fit the coercivity spectra in the component analysis of the IRM using the MAX UnMix method (Maxbauer et al., 2016). Component 1 with low coercivity (mostly <100 mT) represents magnetite;

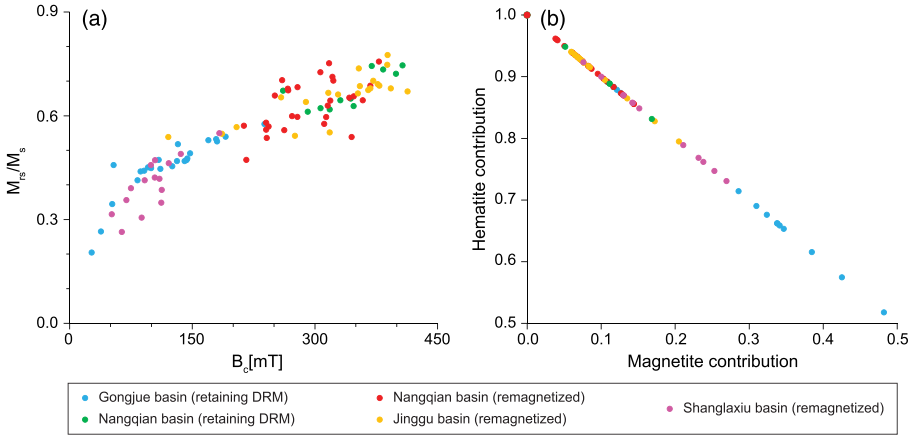

Figure 5. Plot of M_{rs}/M_s ratio versus B_c value (a) and hematite contribution versus magnetite contribution from the IRM component analysis (b) of the measured red beds samples from the Gongjue, Nangqian, Shanglaxiu, and Jinggu basins.

its contribution is mostly <40%. Component 2 with high coercivity (>400 mT) represents hematite; its contribution is mostly >60% (Table S2). Samples from the Nangqian Basin have rectangular hysteresis loops (Figures 4c and 4d) and high B_c (213–407 mT) and B_{cr} (368–523 mT) values (Table S1). The two components used to fit the IRM coercivity spectra represent magnetite and hematite (Figures 4c and 4d), respectively. The contribution of hematite to the IRM is above 90% for most samples (Table S2). Samples from the Shanglaxiu Basin have "wasp-waisted" hysteresis loops (Figures 4e and 4f). The B_c values are relatively low (51–183 mT), and the B_{cr} values are high (346–467 mT) (Table S1). The contribution of magnetite to the IRM varies from 10% to 33%, whereas the contribution of hematite is 67–90% (Table S2). Most samples from the Jinggu Basin have rectangular hysteresis loops (Figure 4h) and high B_c (258–413 mT) and B_{cr} (404–600 mT) values (Table S1), indicating the dominance of hematite as the magnetic carrier (Özdemir & Dunlop, 2014). IRM component analysis reveals that the contribution of hematite is >90% in these samples. In contrast, a few samples have "wasp-waisted" hysteresis loops and relatively lower B_c values (120–204 mT) (Figure 4g; Table S1), indicating a higher concentration of magnetite within them. This is further supported by the results of IRM component analysis, which indicate magnetite contributes ~20% to the IRM (Table S2). In general, hysteresis measurements indicate that magnetite and hematite are the dominant magnetic carriers in red beds from the four basins. Higher B_c values are associated with higher remanent saturation (M_{rs}) to saturation magnetization (M_s) ratios for the analyzed samples (Figure 5a). Samples from the Gongjue and Shanglaxiu basins have comparatively lower B_c values and M_{rs}/M_s ratios, and higher magnetite concentrations, compared to these of samples from the Nangqian and Jinggu basins (Figures 5a and 5b). We have to point out here that contribution of detrital magnetite to the NRM in remagnetized red beds may have been overestimated by the IRM component analysis. Fine-grained hematite (<180 nm), as indicated by the following low-temperature measurements discussed in the next section, has low coercivity (Özdemir & Dunlop, 2014), overlapping with that of magnetite. Component 1 may represent mixture of magnetite and fine-grained hematite in some samples.

4.3. Low-Temperature Magnetic Properties

4.3.1. Low-Temperature Cycling of Room-Temperature Saturation IRM

We subjected 30 samples (8 from the Gongjue Basin, 4 from the Nangqian Basin, 12 from the Jinggu Basin, and 6 from the Shanglaxiu Basin; Table S3) to low-temperature cycling of room temperature saturation isothermal remanent magnetization (RTSIRM). A 2.5 T field was induced to isothermally magnetize the samples at 300 K, and then samples were cooled to 20 K and rewarmed to room temperature with magnetization measured in zero field. The RTSIRM cooling curves of all samples from the Gongjue and Jinggu basins, and of most samples from the Nangqian Basin, show a decrease in remanence on cooling (Figures 6a–6d, 6g, and 6h). The RTSIRM warming curves of these samples are characterized by an increase in magnetization, followed by a decrease at varying temperatures. In contrast, the RTSIRM cycling curves of a few Type A

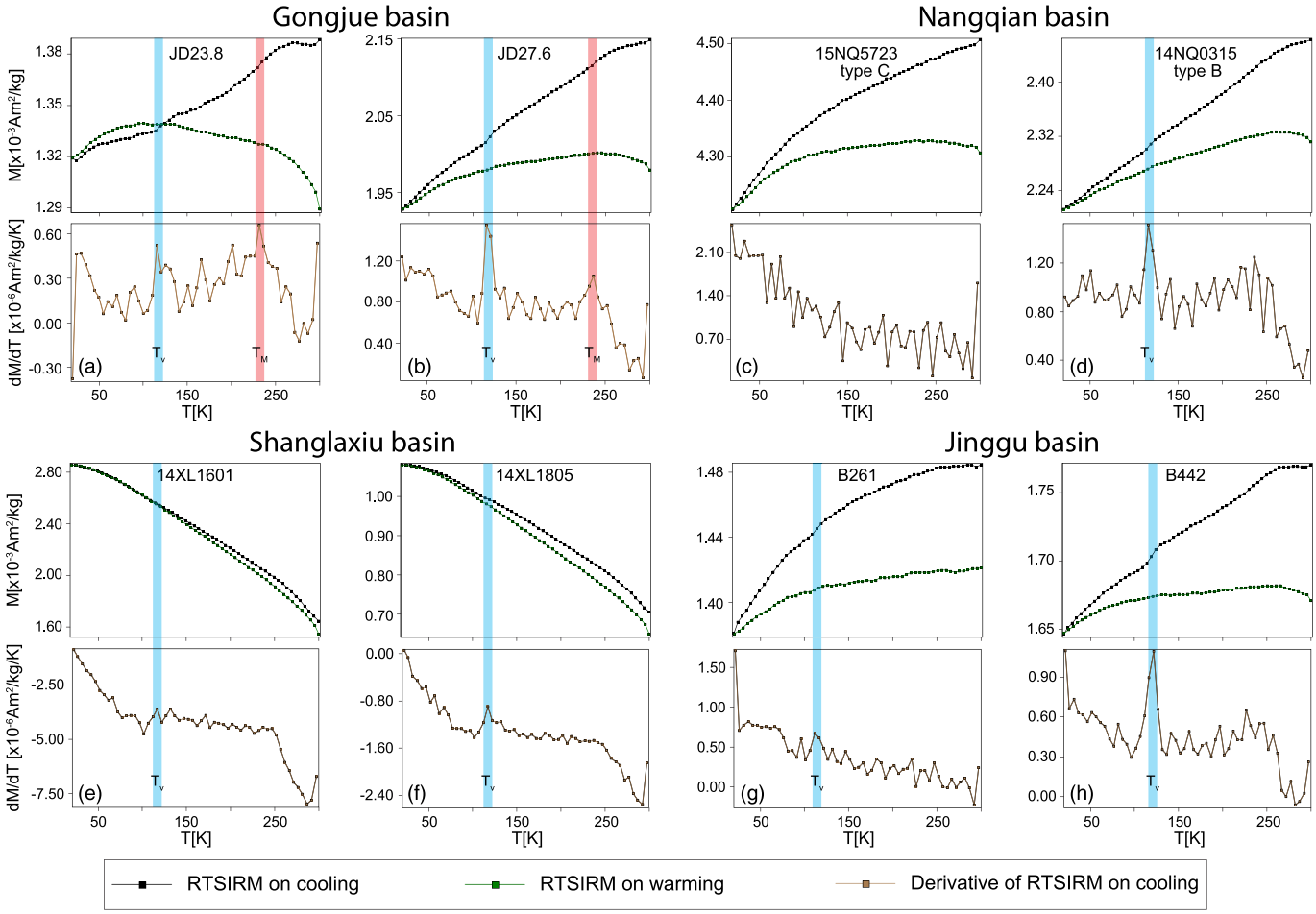

Figure 6. Low-temperature RTSIRM cycling curves at zero field and corresponding derivatives of the RTSIRM cooling for representative red bed samples from the Gongjue (a, b), Nangqian (c, d), Shanglaxiu (e, f), and Jinggu (g, h) basins. Blue and red bars represent the range for the Verwey transition of magnetite and the Morin transition of hematite, respectively.

samples from the Nangqian Basin and all of the samples from the Shanglaxiu Basin show a monotonic increase in magnetization on cooling and a decrease on warming with little loss of remanence due to the cycling (Figures 6e, 6f, and 8b), indicative of a significant goethite concentration in these samples (Rochette & Fillion, 1989). Two remarkable drops in magnetization can be identified at ~240 and ~120 K in the RTSIRM cooling curves of the Gongjue samples (Figures 6a, and 6b). They are more apparent in the derivatives of the RTSIRM cooling curves and represent the Morin transition in hematite and the Verwey transition in magnetite (Özdemir et al., 1993, 2008). The Morin transition cannot be recognized in samples from Nangqian, Shanglaxiu, and Jinggu basins, whereas the Verwey transition is displayed in most samples (Figures 6c–6h).

4.3.2. Low-Temperature SIRM Warming

Samples for the low-temperature SIRM warming measurements are the same as those for the RTSIRM cycling experiments. Field-cooled (FC) remanence was imprinted by cooling the samples from 300 to 20 K in a 2.5 T field; zero-field-cooled (ZFC) remanence was imparted at 20 K by application and removal of a 2.5 T field after cooling the samples from 300 to 20 K in a zero field. Results of low-temperature SIRM warming experiments after ZFC and FC treatments for samples from the four basins are presented in Figure 7. Both the ZFC and FC curves show a continuous decay in remanence during warming to room temperature, indicating progressive unblocking of nanoparticles of the magnetic phases (i.e., hematite, goethite, magnetite, and possibly maghemite). The Verwey transition is apparent in most samples, indicating the presence of nearly stoichiometric magnetite. The FC curves are higher than the ZFC curves, but the difference between

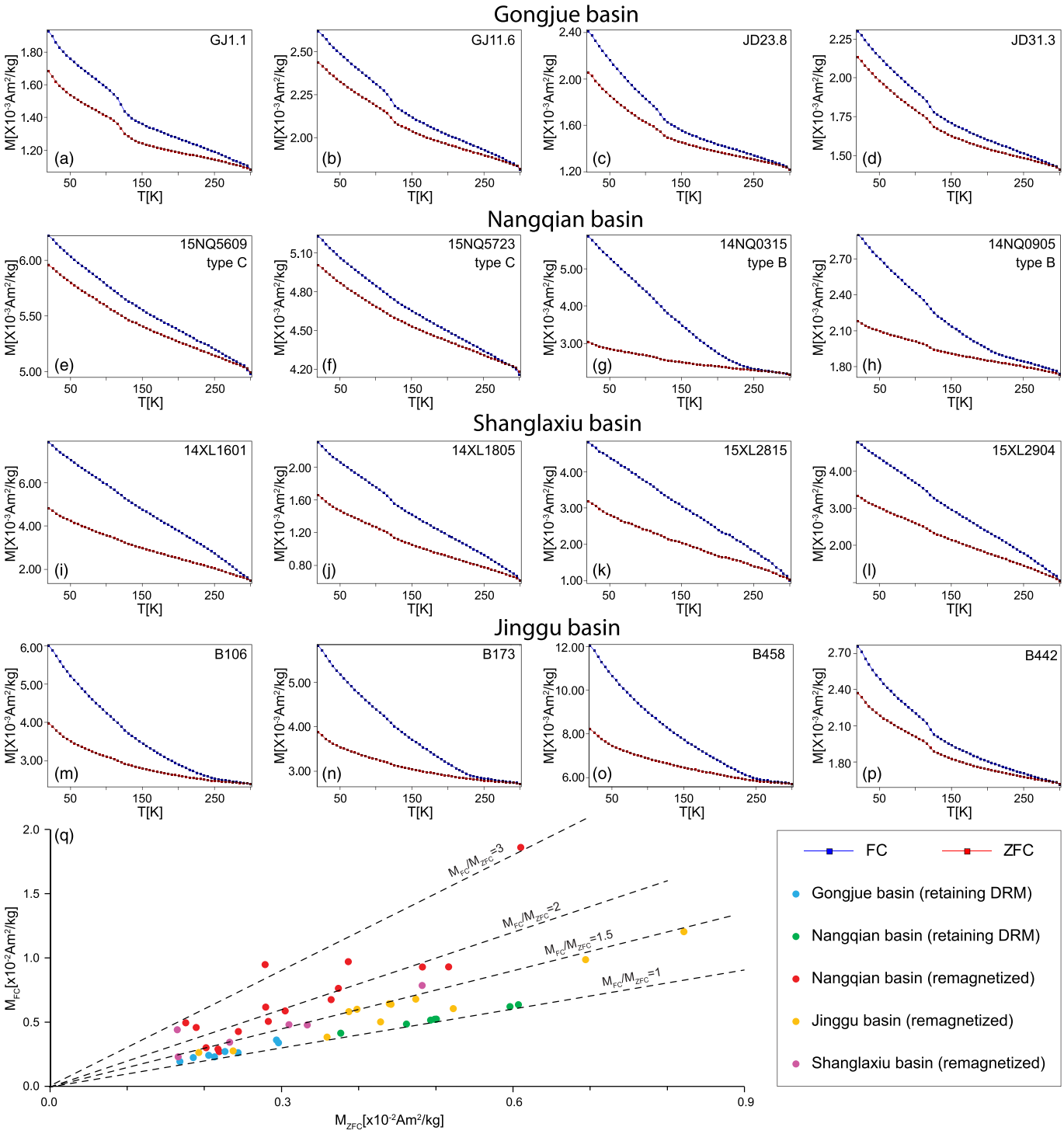

Figure 7. Low-temperature SIRM warming curves in zero field after ZFC and FC treatments in a 2.5 T field of representative red beds samples from the Gongjue (a–d), Nangqian (e–h), Shanglaxiu (i–l), and Jinggu (m–p) basins. FC and ZFC curves of samples retaining the DRM (a–f) are close to each other, whereas most remagnetized samples (g–o) have widely separated FC and ZFC curves. (q) Magnetizations of the FC versus ZFC curves at 20 K of the measured red beds samples from the four basins.

the two is very small for samples retaining primary NRM from the Gongjue and Nangqian basins (Figures 7a–7f), whereas the FC remanence is much stronger than the ZFC remanence for most remagnetized samples from the Nangqian, Shanglaxiu, and Jinggu basins (Figures 7g–7o), which is

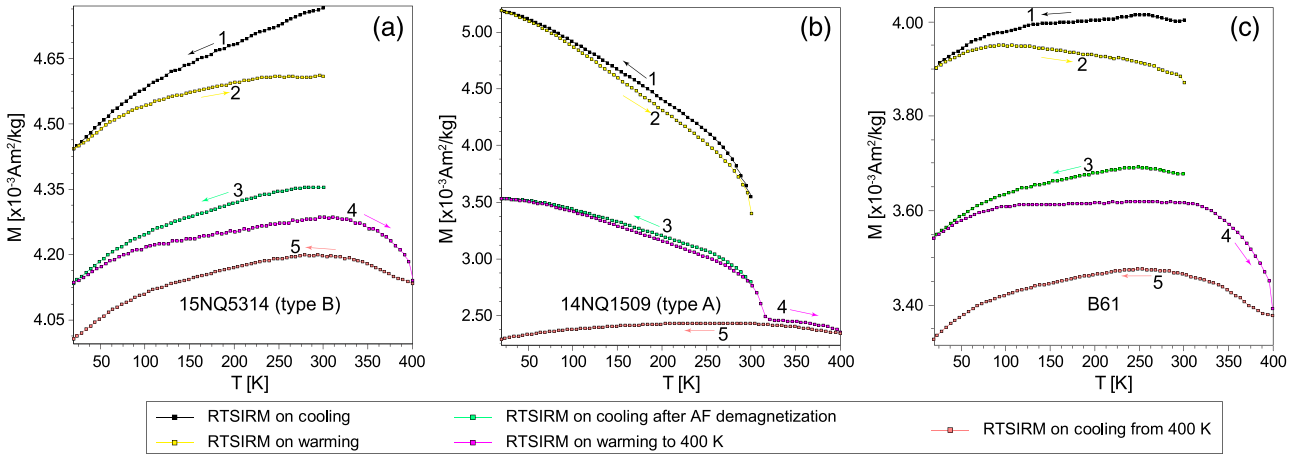

Figure 8. Testing of goethite in representative remagnetized samples from the Nangqian Basin (a and b) and Jinggu Basin (c) with multiple low-temperature cycles of the RTSRIM. Numbers represent the sequence of measurements for the tests; further explanation is in the main text.

usually caused by goethite (Guyodo et al., 2003). The ratio of FC remanence to ZFC remanence (M_{FC}/M_{ZFC}) at 20 K is <1.2 for samples retaining primary NRM from the Gongjue and Nangqian basins, but M_{FC}/M_{ZFC} varies from 1.23 to 3.40 for the remagnetized Nangqian samples, from 1.39 to 2.67 for the remagnetized Shanglaxiu samples, and from 1.37 to 1.51 for most remagnetized Jinggu samples (Figure 7q; Table S3). It is also worth noting that four of the 12 tested remagnetized Jinggu samples do not have widely separated FC and ZFC curves with M_{FC}/M_{ZFC} values at 20 K of 1.07–1.17 (Figures 7p–7q; Table S3).

4.3.3. Low-Temperature Cycling for Testing Goethite

A series of low-temperature remanence measurements are commonly combined to detect goethite (e.g., Guyodo et al., 2006). We applied this test to two remagnetized samples (15NQ5314 and 14NQ1509) from the Nangqian Basin and one remagnetized sample (B61) from the Jinggu Basin with the results presented in Figure 8. RTSIRM cycling curves of Sample 15NQ5314 show a continuous decrease in magnetization on cooling and an increase in magnetization on warming, without a Verwey transition and with a net loss of magnetization. The following AF demagnetization with a peak field of 200 mT removed ~5.5% of the total magnetization, which can be attributed to fine-grained hematite with low coercivity at room temperature, as well as any ferromagnetic magnetite and maghemite that may be present. Cycling curves of the AF-demagnetized sample between 300 and 20 K show continuous decreases and increases on cooling and warming, respectively. Above 300 K, the warming curve is characterized by a remarkable decrease in magnetization up to 400 K, which is the Néel temperature of goethite. The last measurement of the sample on cooling from 400 to 20 K (curve 5) collects the behavior of the AF-resistant hematite. Magnetization of the sample at 300 K in this measurement represents the contribution of large hematite grains with unblocking temperature >400 K, which is 91.1% of the initial magnetization at room temperature. The goethite contribution to remanence at room temperature can thus be estimated of ~3.4%. However, this value should only be treated as an upper limit for goethite because some fine hematite grains with low unblocking temperature may also be demagnetized during warming from 300 to 400 K. Sample 14NQ1509 shows a large increase in magnetization on cooling and a decrease on warming with little net loss of remanence due to the cycling, which are characteristic features for goethite (Rochette & Fillion, 1989). AF demagnetization removed 17.6% of the magnetization at room temperature, which should also be carried by fine-grained hematite because the Verwey transition is not present on the cycling curves. The following warming curve from 20 to 400 K shows a sharp drop in magnetization between 300 and 330 K, indicating that the size of the goethite grains is small. With the same method as described above, we estimate a value of ~10.9% as the contribution of goethite to the magnetization at room temperature. Sample B61 behaves similarly to Sample 14NQ5314. The difference is that magnetite is present as shown by the Verwey transition on the RTSIRM cycling curves. After AF demagnetization, the Verwey transition of magnetite is not seen in the subsequent temperature sweeps. The estimated goethite contribution to the magnetization at 295 K is ~5.5%.

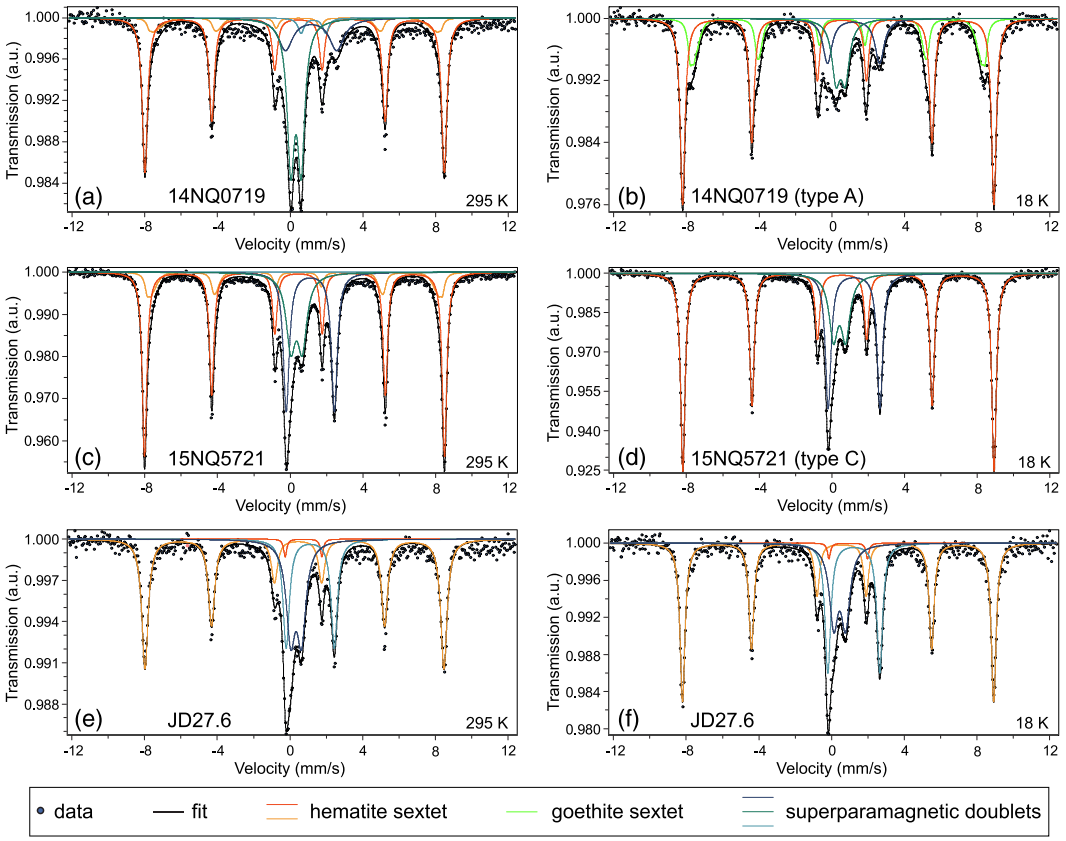

Figure 9. Mössbauer spectra for red bed samples from the Nangqian (a–d) and Gongjue (e and f) basins. Each sample was measured at both 295 and 18 K. Dots with the black lines are data and model fits. Red and orange sextets are the fits diagnostic of hematite; green sextet is representative of goethite. The central peaks are composed of superposed doublets dominated by Fe^{3+}. Sample 14NQ0719 is remagnetized, whereas Samples 15NQ5721 and JD27.6 retain the primary NRM.

5. Mössbauer Spectra

The technique of Mössbauer spectroscopy has long been used as a gold standard for determining Fe^{3+} and Fe^{2+} in solid materials, including geological materials. Mössbauer spectra were collected from three crushed bulk samples, of which 14NQ0719 is a remagnetized sample from the Nangqian basin and 15NQ5721 and JD27.6 are samples retaining primary NRM from the Nangqian and Gongjue basins, respectively. The measurements for each sample were made at both 295 and 18 K. The combination of room temperature and low-temperature measurements allows better discrimination of the magnetic minerals present and their state at room temperature (thermally stable, with an absorption sextet, or superparamagnetic, with a doublet) (Dyar et al., 2006). Bulk hematite and goethite have respective magnetic hyperfine fields of 51.8 and 38.2 T at room temperature, and 54.2 and 50.4 at 4.2 K (Murad & Cashion, 2004). Goethite with particle sizes below about 15–20 nm exhibit superparamagnetic doublets at room temperature, and the 300 K Mössbauer blocking diameter for hematite is about 8 nm (Murad & Cashion, 2004).

The Mössbauer spectrum at 295 K for 14NQ0719 can be fitted with two sextets and three doublets (Figure 9a). The main sextet with a magnetic hyperfine field (B_{HF}) of 51.12 T has parameters similar to those of hematite at room temperature, and the minor one, with B_{HF} = 49.81 T, possibly represents fine-grained hematite (Dyar et al., 2006). Modeling of the spectra reveals that the 52.52% of the iron resides in hematite, with the rest in paramagnetic or superparamagnetic particles (Table S4). At 18 K, the Mössbauer spectrum of 14NQ0719 is also fitted with two sextets and two doublets (Figure 9b). Parameters of one sextet fitted with a smaller magnetic B_{HF} of 50.35 T are close to those of goethite at 18 K, so this sextet possibly represents goethite. The other sextet has B_{HF} of 53.15 T at 18 K is interpreted to be hematite. The appearance of a

significant amount of goethite and the dramatic decrease in the (super)paramagnetic doublets in this sample at 18 K indicate that most of the goethite grains are superparamagnetic at room temperature but are blocked at 18 K. For Sample 15NQ5721, the Mössbauer spectrum at 295 K can be fitted with two sextets and two doublets (Figure 9c). Both of the sextets are interpreted to be hematite, containing 57.27% of the total iron residing in it. At 18 K, this sample is fitted by one sextet (representing hematite) and two doublets (Figure 9d). The modeled hematite contribution slightly increases to 59.7%. For Sample JD27.6, the Mössbauer spectrum at both 295 and 18 K can be fitted by one sextet and three doublets (Figures 9e and 9f). The sextet corresponds to hematite at both temperatures, and its contribution increases from 47.7% at 295 K to 50.2% at 18 K (Table S4). All the three samples show slight increase in the content of the hematite sextet(s) at 18 K, and this is likely due to blocking of the smallest nanoparticles of hematite at low temperature (Bødker et al., 2000). Moreover, both 14NQ0719 and 15NQ5721 have a sextet representing fine-grained hematite at 295 K, whereas JD27.6 does not have it. This may be related to the fact that 14NQ0719 and 15NQ5721 record overprints carried by fine-grained hematite, whereas JD27.6 does not suffer from overprinting.

6. SEM Observation and EDS Analysis

We applied SEM observation, and EDS analyses were done on 25 samples (6 from the Gongjue Basin, 6 from the Nangqian Basin, 3 from the Shanglaxiu Basin, and 10 from the Jinggu Basin) to estimate the diagenetic conditions of the magnetic carriers, and the results are presented in Figures 10 and S1. Detrital titanomagnetite with solid-state exsolution features and hematite are abundant in the Gongjue samples (Figures 10a–10d). These magnetic grains are a few to tens of microns in size and are altered only rarely. For the Nangqian samples, plate-like detrital hematite particles with a size of a few microns can be observed in those retaining the DRM (Figure 10e). Detrital titanomagnetite suffered from strong alteration and fine-grained authigenic needle-like, thin-layered, and amorphous pore-filling hematite is omnipresent (Figures 10f–10h). Authigenic magnetite/maghemite pseudomorphic after early diagenetic framboidal or euhedral pyrite is also observed (Huang, Jackson, Dekkers, Solheid, et al., 2019). In samples from the Shanglaxiu Basin, most detrital titanomagnetite grains are extensively altered with iron largely leached from the lattice (Figures 10j, 10o, and 10p); a few unaltered titanomagnetite grains are also present (Figures 10i and 10n). However, the dominant magnetic mineral phase is authigenic fine-grained hematite, with some hematite grains are pseudomorphic after pyrite (Figure 10i), while some others look like alteration products of detrital hematite (Figure 10k) or Fe-bearing silicates (e.g., biotite and clay minerals) (Figure 10o), and yet others are pore-filling cements between silicates (e.g., quartz and feldspar) (Figure 10m). The dominant magnetic mineral phase in the Jinggu samples is also authigenic hematite, most of which occurs as needle/plate-like and fine particles (Figures 10q and 10s–10u); detrital hematite is hardly observed (Figure 10r). Iron in the authigenic hematite is mainly derived from alteration of detrital Fe-bearing silicates and titanomagnetite (Figures 10t and 10v–10x). Detrital titanomagnetite grains are largely altered and replaced by rutile and authigenic hematite (Figures 10v and 10w). In summary, detrital titanomagnetite and hematite in red beds from the Gongjue Basin are rarely altered, whereas detrital magnetic minerals in the remagnetized red beds from the Nangqian, Shanglaxiu, and Jinggu basins are severely altered with their iron leached and deposited as authigenic hematite. It is worth noting that hematite and goethite cannot be discriminated under SEM observations and EDS analysis, but these minute needle-like iron oxides in remagnetized red beds (Figures 10m, 10q, 10s, and 10u) may be goethite, or hematite pseudomorphic after goethite (Weibel & Grobety, 1999).

7. Discussion

7.1. Mechanisms of Remagnetization in Red Beds

Remagnetization of red beds is often induced by CRM acquisition during replacement of precursor detrital magnetic minerals by authigenic magnetic phases, as in the Appalachian red beds and red beds from the South China, Sibumasu, and Indochina blocks (e.g., Huang & Opdyke, 2015; Jiang et al., 2017; Tsuchiyama et al., 2016; van der Voo & Torsvik, 2012). Our rock magnetic measurements (Figures 3–9) and SEM observations (Figure 10) show that the magnetic carriers of the remagnetized red beds from the Nangqian (Types A and B) Shanglaxiu and Jinggu basins are dominated by authigenic magnetic phases (hematite, goethite, and little magnetite), whereas the detrital magnetic minerals (titanomagnetite and

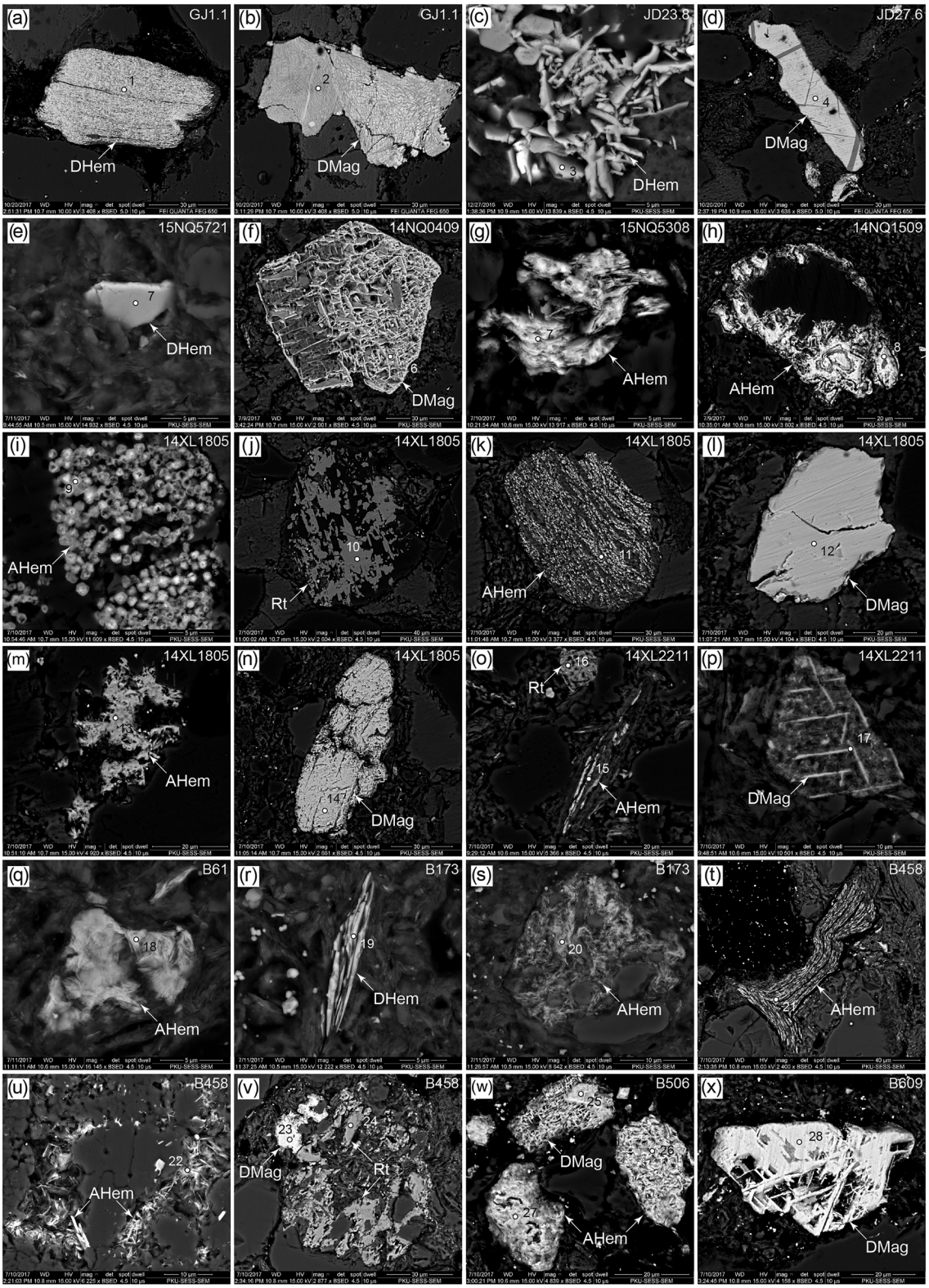

Figure 10. SEM backscattered electron images of samples from the Gongjue, Nangqian, Shanglaxiu, and Jinggu basins. DHem = detrital hematite; AHem = authigenic hematite; DMag = detrital magnetite; Rt = rutile. (a–d) From samples retaining a DRM from the Gongjue Basin; (e) from a Type C sample retaining a DRM from the Nangqian Basin; (f–h) from remagnetized Types A and B samples from the Nangqian Basin; (i–p) from remagnetized samples from the Shanglaxiu Basin; and (q–x) from remagnetized samples from the Jinggu Basin. Dots represent spots for EDS analysis with the results presented in Figure S1.

hematite) are severely altered and rarely preserved. In contrast, authigenic magnetic phases are rare, and detrital magnetic minerals are seldomly and only moderately altered in red beds that retain the DRM from the Gongjue and Nangqian (Type C) basins, respectively (Figures 3–10). These results strongly suggest that breakdown of the DRM carried by detrital magnetic minerals and acquisition of CRM carried by authigenic magnetic phases is the principal mechanism for remagnetization of the studied red beds. Growth of the authigenic magnetic phases was at the expense of the detrital Fe-bearing phases during the late diagenesis. Leached iron from the detrital Fe-bearing minerals and early diagenetic pyrite was first oxidized and probably formed poorly crystalline ferrihydrite, which transformed to more thermodynamically stable and more crystalline goethite and hematite simultaneously at neutral pH (e.g., Das et al., 2011; Jiang et al., 2016). Small goethite grains (<10 nm) are metastable and may dehydrate and transform to nanocrystalline hematite (Till et al., 2015), whereas large goethite grains (>10 nm) are stable and well preserved through geologic time.

Authigenic magnetite/maghemite pseudomorphic after pyrite is probably rare considering the redox conditions that prevailed (Figure 10). Authigenic goethite is mostly fine grained and the larger grains unblock up to its Néel temperature of 400 K (Figures 8 and 9). Therefore, CRM in the remagnetized red beds mostly resides in authigenic hematite. The CRM in remagnetized samples from the Nangqian (Types A and B), Shanglaxiu, and Jinggu basins was gradually removed from room temperature to the Néel temperature of hematite of 680°C (Figure 2), corresponding to hematite grain sizes ranging from ~30 to >600 nm based on the hematite grain volume and unblocking temperature relationship following from Néel theory (Swanson-Hysell et al., 2019). Some remagnetized samples from the Jinggu Basin were completely demagnetized by 630°C (Figures 2m and 2p), indicating that the size of their authigenic hematite within it is up to 300 nm. In contrast, CRM of Type C samples from the Nangqian Basin is erased from 300°C up to 600°C (Figure 2g; Huang, Jackson, Dekkers, Solheid, et al., 2019), which means that the authigenic hematite is <120–240 nm. In samples retaining the DRM from both the Gongjue and Nangqian basins, DRM carried by detrital hematite unblocks between 600°C and 680°C (Figures 2a–2d, 2g, and 2h), corresponding to hematite grain sizes of >240 nm. These observations support that hematite carrying the CRM has a wide distribution of grain size and unblocking temperature spectra, while hematite carrying the DRM is usually coarse and has confined unblocking temperature spectrum due to hydrodynamic sorting (Jiang et al., 2015; Swanson-Hysell et al., 2019). The contribution of detrital (titano)magnetite to the NRM is low in the remagnetized red beds (Figure 4), and its signal is probably swamped by the authigenic hematite with a broad unblocking temperature spectra.

Elevated temperature related to burial or magmatism could promote or even induce diagenesis. Alteration of detrital Fe-bearing minerals, precipitation of ferrihydrite from leached iron, and transformation of ferrihydrite to hematite and goethite would be significantly accelerated at high temperature. Low-temperature thermochronolgic studies on the Gongjue and Nangqian basins indicate that detrital apatite (U-Th-Sm)/He ages with a closure temperature of 60–80°C (Farley, 2000) were reset but detrital zircon (U-Th)/He ages with a closure temperature of 160–180°C (Reiners et al., 2004) were not reset (unpublished data from Dr. Lin Li and us). No thermochronologic data from the Shanglaxiu and Jinggu basins are known to us, but their surrounding areas have thermal histories similar to those of the Gongjue and Nangqian basins (Dai et al., 2013; Nie et al., 2018). These results suggest that the four basins studied here were possibly heated up to ~100°C during burial. Besides, magmatic activity could be another source of heat. Red beds in the Nangqian Basin were intruded by magmatic rocks at 38–37 Ma (Spurlin et al., 2005). The remanence direction of the remagnetized red beds is similar to that of the primary NRM of the magmatic rocks (Roperch et al., 2017). More importantly, the extent of overprinting is closely related to the distance of the red beds to magmatic bodies. This led us to interpret that heating related to magmatism promoted diagenesis and induced remagnetization of red beds in the Nangqian Basin (Huang, Jackson, Dekkers, Solheid, et al., 2019). Volcanic rocks at 51–49 Ma are also present in the Shanglaxiu Basin (Spurlin et al., 2005), but the volume of volcanic bodies intruding the red beds is very small (Figure 1e). Besides, the remagnetization direction of the red beds is distinct from that of the primary NRM of the volcanic rocks (Roperch et al., 2017). Thus, heating related to local magmatism cannot be the reason for the remagnetization. Magmatism is absent in the Jinggu Basin, and thus, there must be other reasons inducing the later diagenesis and remagnetization.

Diagenesis is often assisted by fluids. Circulation of orogenic fluids, pumped by tectonically induced overpressure, or gravity, is one of the main reasons for chemical remagnetization in a variety of rocks (e.g.,

Elmore et al., 2012). This has been used to explain the remagnetization of the Jinggu red beds (Li et al., 2017). They contain organic matter as becomes evident in red beds from the Jinggu Basin under microscopic observations of thin sections and during χ-T measurements (some crushed samples turned to black after heating up to 700°C). The organic matter is more likely related to basinal hydrocarbon migration, which was inferred to be linked to the formation of the local Denghaishan copper deposit in the early Oliogence (Chen, 2012). Indeed, mineralization related to hydrothermal fluid migration during late Eocene to Oligocene time is omnipresent in the southeast margin of the Tibetan Plateau (Deng et al., 2014). Therefore, for the Jinggu red beds, following Cox et al. (2005), we propose that hydrocarbon migration, perhaps driven through the rocks by regional deformation, caused dissolution of the detrital magnetic minerals and Fe-bearing silicates under reductive conditions in the first stage. Subsequently, circulation of oxidizing meteoric fluids during the second stage induced oxidation of the leached iron and precipitation of authigenic magnetic phases. Red beds from the Shanglaxiu Basin do not contain organic matter, and it is likely that the remagnetization was induced by circulation of oxidizing meteoric fluids, similar to an episode of remagnetization in the surrounding Triassic carbonate rocks (Huang, Jackson, Dekkers, Zhang, et al., 2019). The concentration of (titano)magnetite within these rocks is high (Figure 5b), and it should have been even higher before the diagenesis. This means that much iron could have been leached from detrital (titano)magnetite and other Fe-bearing minerals during the circulation of oxidizing fluids and transformed to authigenic magnetic phases. Grain size of the red beds may have been a controlling factor for fluid circulation: coarser grains mean higher porosity in the rocks, making it easier for the fluid to migrate. Both the Jinggu and Shanglaxiu red beds are coarse sandstone and siltstone, whereas red beds from the Nangqian Basin are dominated by mudstones. Thus, lithological difference permitted circulation of fluid through red beds from the Jinggu and Shanglaxiu basins but prohibited much external fluid circulation in the Nangqian red beds. This further supports that fluid circulation induced remagnetization of red beds in the Jinggu and Shanglaxiu basins but heating related to magmatism is considered the main cause for remagnetization of the Nangqian red beds. Fluid circulation seems more effective in remagnetizing red beds than heating. DRM is preserved in some Nangqian samples, but it was completely replaced by CRM in the Shanglaxiu and Jinggu samples. One possible explanation is that heating related to magmatism is shorter lived than fluid circulation.

7.2. Criteria for Diagnosing Remagnetization in Red Beds

The wide distribution of unblocking temperatures of the CRM leads to the concave or linear shape of the thermal decay curves in remagnetized red beds, which contrasts with the convex thermal decay curves of red beds retaining DRM (Jiang et al., 2015). This remarkable difference has been widely used to distinguish CRM from DRM in red beds and works well for samples revealing one magnetic component during thermal demagnetization, such as samples from the Gongjue Basin, Type A samples from the Nangqian Basin, and samples from the Shanglaxiu and Jinggu basins (Figure 2). Attention should be paid here to red beds with high concentration of detrital titanomagnetite. It is worth noting that this characteristic is more clearly displayed in the thermal decay curves of the remanence than susceptibility. The χ-T curves of the Gongjue samples are similar to those of the Shanglaxiu samples (Figure 3), but their thermal demagnetization curves of the NRM are significantly distinct (Figure 2). This is probably due to the high titanomagnetite content in samples from both basins (Figures 5a and 5b). However, this criterion for discriminating CRM from DRM can be problematic when the red bed samples reveal multiple NRM components. Evaluating whether the high-temperature component is a DRM is difficult in such cases.

In the previous work on red beds from the Nangqian Basin (Huang, Jackson, Dekkers, Solheid, et al., 2019), we have found that remagnetized samples (Types A and B) contain large amounts of nanoscaled goethite, whereas little goethite exists in samples retaining the DRM (Type C). This is further supported by the supplementary low-temperature rock magnetic and Mössbauer spectrum data of the Nangqian red beds presented in this research (Figures 6–9). Nanogoethite is also detected in most remagnetized red beds from the Shanglaxiu and Jinggu basins, whereas it is absent in the red beds from the Gongjue Basin (Figures 5–7). Separation between the FC and ZFC warming curves almost certainly indicates the existence of nanogoethite. In general, the causes for FC-ZFC separation include induced (1) anisotropy produced in magnetite by the cooling field, which is not the case here in red beds, and nonsaturation of hard antiferromagnetic remanence in the 2.5 T MPMS field. Magnetite's presence is subordinate at best in the red beds studied

here, so Option 1 is not applicable. The second option is well known for goethite and for siderite ($FeCO_3$). The absence of a sharp drop of the remanence at 34 K precludes the existence of siderite in our red beds. The only other minerals known for having FC-ZFC separation are the FeOOH forms other than goethite (akaganéite, lepidocrocite, and feroxyhyte), of which the first two are generally thought to be paramagnetic and the third to be usually superparamagnetic at room temperature. We note that four of the 12 measured samples from the Jinggu Basin do not show a significant separation of the FC-ZFC curves with M_{FC}/M_{ZFC} values at 20 K of 1.07–1.17, similar to that of the samples retaining the DRM from the Gongjue and Nangqian basins (Figure 5c). This might be caused by dissolution of goethite in an acid environment created during degradation of the organic matter within these samples. Moreover, the goethite test on a sample from the Jinggu Basin (Figure 8c) and the Mössbauer spectrum of a sample from the Gongjue Basin (Figures 9e and 9f) further confirm presence of nanogoethite in the remagnetized red beds, and its absence in red beds retaining the DRM. Goethite is commonly found as a surface weathering product, but this is not the case here because weathered surface was avoided in our sample collection and goethite is only detected in remagnetized red beds. Therefore, although goethite has little contribution to the NRM, it is a byproduct and a sensitive indicator of the later diagenesis in red beds, similar to the presence of superparamagnetic magnetite/maghemite in remagnetized carbonates (e.g., Jackson & Swanson-Hysell, 2012), and thus can be used as a criterion for detecting remagnetization in red beds. Trace amounts of goethite have been identified in remagnetized Jurassic-Cretaceous red beds by thermal demagnetization of the composite IRMs (Tsuchiyama et al., 2016; Yamashita et al., 2011), which further suggest the universal existence of goethite in remagnetized red beds. We emphasize here that goethite in remagnetized red beds can best be detected by low-temperature measurements because it is fine grained.

Petrographic investigations, including SEM and transmission electron microscopy observations, are valuable for diagnosing remagnetization in red beds. We have observed large amounts of hematite grains that are euhedral (plate/needle-like), amorphous, or pseudomorphic after pyrite and biotite in remagnetized red beds (Figure 10), which strongly suggests that they have an authigenic origin. Their sizes are mostly below 1 micron (Figure 10), corresponding well to their rock magnetic properties of low unblocking temperatures and a widely distributed unblocking temperature spectrum. SEM observations have also shown intensive alteration of detrital (titano)magnetite, hematite, and detrital Fe-bearing silicates (Figure 10), which explains the source of the iron in the authigenic hematite. In contrast, SEM observations have confirmed that detrital (titano)magnetite and hematite are well preserved in red beds retaining the DRM (Figure 10) and that alteration of magnetic minerals is only weak. Thus, SEM observations have helped us to identify the mechanisms of remagnetization in red beds. They provide independent constraints on diagenetic conditions of magnetic phases, which—when integrated with the rock magnetic features including unblocking temperature spectra and goethite concentration—can give us an unequivocal constraints on the origin of NRM in red beds. Once the primary origin of the NRM is confirmed, paleomagnetic results from red beds can be used for geologic interpretations after correction of potential inclination shallowing (Bilardello & Kodama, 2010; Tauxe & Kent, 2004).

8. Conclusions

Erroneous interpretation of the magnetization of red beds (CRM vs. DRM) often leads to controversial geologic reconstructions. In this research, we applied multiple rock magnetic measurements, Mössbauer spectrum experiments, and SEM and EDS analyses to red beds from four Cenozoic basins on the eastern Tibetan Plateau. Our results consistently show that magnetic carriers of red beds retaining the DRM in the Gongjeu and Nangqian basins are dominated by detrital (titano)magnetite and hematite with marginal alteration only. In contrast, remagnetized red beds in the Nangqian, Shanglaxiu, and Jinggu basins are characterized by the massive alteration of detrital Fe-bearing phases and formation of large amounts of authigenic hematite and goethite during strong later diagenesis related to thermal anomalies and/or fluid circulation. The authigenic hematite has a broad grain size distribution and a wide spectrum of unblocking temperatures; grains are typically smaller and unblocking temperatures lower than those of the detrital hematite. Isolation of the DRM in red beds thus depends on the separation of authigenic and detrital hematite in terms of grain size, through its unblocking temperature. Our studies support that thermomagnetic behaviors (NRM thermal decay curves and χ-T curves) and the presence of goethite are powerful property-based

criteria for discriminating the CRM from the DRM in red beds. These criteria, when combined with petrographic examinations, can give robust constraints on the NRM origin in red beds.

Data Availability Statement

Data to support this article are available in Figure S1 and Tables S1–S4, which are also deposited in Zenodo (doi:10.5281/zenodo.3899715).

Acknowledgments

W. H. was supported by three visiting research fellowships from the Institute for Rock Magnetism (IRM) at the University of Minnesota, which is funded by the Instruments and Facilities program of NSF. L. D. was support by the National Natural Science Foundation of China (Grant No. 41988101). Dr. Pierrick Roperch and Dr. Guillaume Dupont-Nivet are especially appreciated for sharing the samples and their thermal demagnetization data. We are grateful to Dr. Marco Maffione and Dr. Daniel Pastor-Galán for their constructive comments on the manuscript. We also thank associate editor Prof. Aleksey Smirnov for handling the manuscript.

References

Bilardello, D., & Kodama, K. P. (2010). Rock magnetic evidence for inclination shallowing in the early Carboniferous Deer Lake Group red beds of western Newfoundland. *Geophysical Journal International*, *181*(1), 275–289. https://doi.org/10.1111/j.1365-246X.2010.04537.x

Bødker, F., Hansen, M. F., Koch, C. B., Lefmann, K., & Mørup, S. (2000). Magnetic properties of hematite nanoparticles. *Physical Review B*, *61*(10), 6826–6838. https://doi.org/10.1103/PhysRevB.61.6826

Bosboom, R., Dupont-Nivet, G., Grothe, A., Brinkhuis, H., Villa, G., Mandic, O., et al. (2014). Linking Tarim Basin sea retreat (west China) and Asian aridification in the late Eocene. *Basin Research*, *26*, 621–640. https://doi.org/10.1111/bre.12054

Bureau of Geology and Mineral Resources of Yunnan Province (BGMRYP) (1990). Regional Geology of Yunnan Province: Beijing, Geological Publishing House. 726 p.

Chen, D. (2012). On genesis and geologic characteristics of the Denghaishan copper deposit in Jinggu County, Yunnan Province. *Geology of Fujian*, *3*, 6.

Cogné, J. P., Halim, N., Chen, Y., & Courtillot, V. (1999). Resolving the problem of shallow magnetizations of Tertiary age in Asia: Insights from paleomagnetic data from the Qiangtang, Kunlun, and Qaidam blocks (Tibet, China), and a new hypothesis. *Journal of Geophysical Research*, *104*(B8), 17,715–17,734. https://doi.org/10.1029/1999JB900153

Cox, E., Elmore, R. D., & Evans, M. (2005). Paleomagnetism of Devonian red beds in the Appalachian plateau and valley and ridge provinces. *Journal of Geophysical Research*, *110*, B08102. https://doi.org/10.1029/2005JB003640

Dai, J., Wang, C., Hourigan, J., & Santosh, M. (2013). Insights into the early Tibetan Plateau from (U–Th)/He thermochronology. *Journal of the Geological Society*, *170*, 2012–2076.

Das, S., Hendry, M. J., & Essilfie-Dughan, J. (2011). Transformation of two-line ferrihydrite to goethite and hematite as a function of pH and temperature. *Environmental Science & Technology*, *45*(1), 268–275. https://doi.org/10.1021/es101903y

Deng, J., Wang, Q., Li, G., & Santosh, M. (2014). Cenozoic tectono-magmatic and metallogenic processes in the Sanjiang region, southwestern China. *Earth-Science Reviews*, *138*, 268–299. https://doi.org/10.1016/j.earscirev.2014.05.015

Dunlop, D. J., & Ödemir, Ö. (1997). *Rock magnetism: Fundamentals and frontiers* (p. 573). Cambridge: Cambridge University Press. https://doi.org/10.1017/CBO9780511612794

Dyar, M. D., Agresti, D. G., Schaefer, M. W., Grant, C. A., & Sklute, E. C. (2006). Mössbauer spectroscopy of Earth and planetary materials. *Annual Review of Earth and Planetary Sciences*, *34*(1), 83–125. https://doi.org/10.1146/annurev.earth.34.031405.125049

Elmore, R. D., Muxworthy, A. R., & Aldana, M. (2012). Remagnetization and chemical alteration of sedimentary rocks. *Geological Society, London, Special Publications*, *371*(1), 1–21. https://doi.org/10.1144/SP371.15

Farley, K. (2000). Helium diffusion from apatite: General behavior as illustrated by Durango fluorapatite. *Journal of Geophysical Research*, *105*(B2), 2903–2914. https://doi.org/10.1029/1999JB900348

Guyodo, Y., LaPara, T. M., Anschutz, A. J., Penn, R. L., Banerjee, S. K., Geiss, C. E., & Zanner, W. (2006). Rock magnetic, chemical and bacterial community analysis of a modern soil from Nebraska. *Earth and Planetary Science Letters*, *251*(1–2), 168–178. https://doi.org/10.1016/j.epsl.2006.09.005

Guyodo, Y., Mostrom, A., Penn, R. L. & Banerjee, S. K. (2003). From nanodots to nanorods: Oriented aggregation and magnetic evolution of nanocrystalline goethite. *Geophysical Research Letters*, *30*(10), 1512. https://doi.org/10.1029/2003GL017021

Horton, B. K., Yin, A., Spurlin, M. S., Zhou, J., & Wang, J. (2002). Paleocene-Eocene syncontractional sedimentation in narrow, lacustrine-dominated basins of east-central Tibet. *Geological Society of America Bulletin*, *114*(7), 771–786.

Huang, K., & Opdyke, N. D. (2015). Post-folding magnetization of the Triassic rocks from western Guizhou and southern Yunnan provinces: New evidence for large clockwise rotations in the Simao Terrane. *Earth and Planetary Science Letters*, *423*, 155–163. https://doi.org/10.1016/j.epsl.2015.05.015

Huang, K., Opdyke, N. D., Li, J., & Peng, X. (1992). Paleomagnetism of Cretaceous rocks from eastern Qiangtang terrane of Tibet. *Journal of Geophysical Research*, *97*(B2), 1789–1799. https://doi.org/10.1029/91JB02747

Huang, W., Jackson, M. J., Dekkers, M. J., Solheid, P., Zhang, B., Guo, Z., & Ding, L. (2019). Nanogoethite as a potential indicator of remagnetization in red beds. *Geophysical Research Letters*, *46*, 12,841–12,850. https://doi.org/10.1029/2019GL084715

Huang, W., Jackson, M. J., Dekkers, M. J., Zhang, Y., Zhang, B., Guo, Z., & Dupont-Nivet, G. (2019). Challenges in isolating primary remanent magnetization from Tethyan carbonate rocks on the Tibetan Plateau: Insight from remagnetized Upper Triassic limestones in the eastern Qiangtang block. *Earth and Planetary Science Letters*, *523*, 115695. https://doi.org/10.1016/j.epsl.2019.06.035

Huang, W., van Hinsbergen, D. J. J., Maffione, M., Orme, D. A., Dupont-Nivet, G., Guilmette, C., et al. (2015). Lower Cretaceous Xigaze ophiolite formed in the Gangdese forearc: Evidence from paleomagnetism, sediment provenance, and stratigraphy. *Earth and Planetary Science Letters*, *415*, 142–153. https://doi.org/10.1016/j.epsl.2015.01.032

Jackson, M., & Swanson-Hysell, N. L. (2012). Rock magnetism of remagnetized carbonate rocks: Another look. *Geological Society, London, Special Publications*, *371*(1), 229–251. https://doi.org/10.1144/SP371.3

Jiang, Z., Liu, Q., Dekkers, M. J., Barrón, V., Torrent, J., & Roberts, A. P. (2016). Control of Earth-like magnetic fields on the transformation of ferrihydrite to hematite and goethite. *Scientific Reports*, *6*, 30395. https://doi.org/10.1038/srep30395

Jiang, Z., Liu, Q., Dekkers, M. J., Tauxe, L., Qin, H., Barrón, V., & Torrent, J. (2015). Acquisition of chemical remanent magnetization during experimental ferrihydrite–hematite conversion in Earth-like magnetic field—Implications for paleomagnetic studies of red beds. *Earth and Planetary Science Letters*, *428*, 1–10. https://doi.org/10.1016/j.epsl.2015.07.024

Jiang, Z., Liu, Q., Dekkers, M. J., Zhao, X., Roberts, A. P., Yang, Z., et al. (2017). Remagnetization mechanisms in Triassic red beds from South China. *Earth and Planetary Science Letters*, *479*, 219–230. https://doi.org/10.1016/j.epsl.2017.09.019

Kruiver, P. P., Dekkers, M. J., & Langereis, C. G. (2000). Secular variation in Permian red beds from Dôme de Barrot, SE France. *Earth and Planetary Science Letters*, *179*(1), 205–217. https://doi.org/10.1016/S0012-821X(00)00104-7

Li, L., Fan, M., Davila, N., Jesmok, G., Mitsunaga, B., Tripati, A., & Orme, D. (2018). Carbonate stable and clumped isotopic evidence for late Eocene moderate to high elevation of the east-central Tibetan Plateau and its geodynamic implications. *Geological Society of America Bulletin*, *131*, 831–844.

Li, S., van Hinsbergen, D. J. J., Najman, Y., Liu-Zeng, J., Deng, C., & Zhu, R. (2020). Does pulsed Tibetan deformation correlate with Indian plate motion changes? *Earth and Planetary Science Letters*, *536*, 116144. https://doi.org/10.1016/j.epsl.2020.116144

Li, S., Yang, Z., Deng, C., He, H., Qin, H., Sun, L., et al. (2017). Clockwise rotations recorded in redbeds from the Jinggu Basin of northwestern Indochina. *Geological Society of America Bulletin*, *129*, 1100–1122. B31637. 1

Lippert, P. C., van Hinsbergen, D. J. J., & Dupont-Nivet, G. (2014). The Early Cretaceous to Present latitude of the central Lhasa-plano (Tibet): A paleomagnetic synthesis with implications for Cenozoic tectonics, paleogeography and climate of Asia. In J. S. Nie, G. D. Hoke, & B. K. Horton (Eds.), *Towards an improved understanding of uplift mechanisms and the elevation history of the Tibetan plateau, Geological Society of America Special Paper* (Vol. 507, pp. 1–21). Boulder, Colorado: Geological Society of America.

Liu, C., Ge, K., Zhang, C., Liu, Q., Deng, C., & Zhu, R. (2011). Nature of remagnetization of Lower Triassic red beds in southwestern China. *Geophysical Journal International*, *187*(3), 1237–1249. https://doi.org/10.1111/j.1365-246X.2011.05196.x

Ma, A., Hu, X., Garzanti, E., Han, Z., & Lai, W. (2017). Sedimentary and tectonic evolution of the southern Qiangtang basin: Implications for the Lhasa-Qiangtang collision timing. *Journal of Geophysical Research: Solid Earth*, *122*, 4790–4813. https://doi.org/10.1002/2017JB014211

Ma, Y., Yang, T., Yang, Z., Zhang, S., Wu, H., Li, H., et al. (2014). Paleomagnetism and U-Pb zircon geochronology of Lower Cretaceous lava flows from the western Lhasa terrane: New constraints on the India-Asia collision process and intracontinental deformation within Asia. *Journal of Geophysical Research: Solid Earth*, *119*, 7404–7424. https://doi.org/10.1002/2014JB011362

Maxbauer, D. P., Feinberg, J. M., & Fox, D. L. (2016). MAX UnMix: A web application for unmixing magnetic coercivity distributions. *Computers & Geosciences*, *95*, 140–145.

Murad, E., & Cashion, J. (2004). *Iron oxides, Mössbauer spectroscopy of environmental materials and their industrial utilization* (pp. 159–188). Norwell, MA: Kluwer Academic Publishers.

Nie, J., Ruetenik, G., Gallagher, K., Hoke, G., Garzione, C. N., Wang, W., et al. (2018). Rapid incision of the Mekong River in the middle Miocene linked to monsoonal precipitation. *Nature Geoscience*, *11*, 944–948. https://doi.org/10.1038/s41561-018-0244-z

Otofuji, Y., Inoue, S., Funahara, S., Murata, F., & Zheng, X. (1990). Palaeomagnetic study of eastern Tibet-deformation of the Three Rivers region. *Geophysical Journal International*, *103*(1), 85–94. https://doi.org/10.1111/j.1365-246X.1990.tb01754.x

Özdemir, Ö., & Dunlop, D. J. (2014). Hysteresis and coercivity of hematite. *Journal of Geophysical Research: Solid Earth*, *119*, 2582–2594. https://doi.org/10.1002/2013JB010739

Özdemir, Ö., Dunlop, D. J., & Berquo, T. S. (2008). Morin transition in hematite: Size dependence and thermal hysteresis. *Geochemistry, Geophysics, Geosystems*, *9*, Q10Z01. https://doi.org/10.1029/2008GC002110

Özdemir, Ö., Dunlop, D. J., & Moskowitz, B. M. (1993). The effect of oxidation on the Verwey transition in magnetite. *Geophysical Research Letters*, *20*(16), 1671–1674. https://doi.org/10.1029/93GL01483

Reiners, P. W., Spell, T. L., Nicolescu, S., & Zanetti, K. A. (2004). Zircon (U-Th)/He thermochronometry: He diffusion and comparisons with $^{40}Ar/^{39}Ar$ dating. *Geochimica et Cosmochimica Acta*, *68*(8), 1857–1887. https://doi.org/10.1016/j.gca.2003.10.021

Rochette, P., & Fillion, G. (1989). Field and temperature behavior of remanence in synthetic goethite: Paleomagnetic implications. *Geophysical Research Letters*, *16*(8), 851–854. https://doi.org/10.1029/GL016i008p00851

Roperch, P., Dupont-Nivet, G., Guillot, S., Goussin, F., Huang, W., Replumaz, A., et al. (2017). Paleomagnetic constraints on early collisional deformation along the eastern margin of the Qiangtang terrane (Tibetan plateau) at 50 and 37 Ma, EGU general assembly conference abstracts, pp. 9476.

Song, P., Ding, L., Li, Z., Lippert, P. C., Yang, T., Zhao, X., et al. (2015). Late Triassic paleolatitude of the Qiangtang block: Implications for the closure of the Paleo-Tethys Ocean. *Earth and Planetary Science Letters*, *424*, 69–83. https://doi.org/10.1016/j.epsl.2015.05.020

Spurlin, M. S., Yin, A., Horton, B. K., Zhou, J., & Wang, J. (2005). Structural evolution of the Yushu-Nangqian region and its relationship to syncollisional igneous activity, east-central Tibet. *Geological Society of America Bulletin*, *117*(9), 1293–1317. https://doi.org/10.1130/B25572.1

Studnicki-Gizbert, C., Burchfiel, B., Li, Z., & Chen, Z. (2008). Early Tertiary Gonjo basin, eastern Tibet: Sedimentary and structural record of the early history of India-Asia collision. *Geosphere*, *4*(4), 713–735. https://doi.org/10.1130/GES00136.1

Swanson-Hysell, N. L., Fairchild, L. M., & Slotznick, S. P. (2019). Primary and secondary red bed magnetization constrained by fluvial intraclasts. *Journal of Geophysical Research: Solid Earth*, *124*, 4276–4289. https://doi.org/10.1029/2018jb017067

Tauxe, L., & Kent, D. V. (2004). A simplified statistical model for the geomagnetic field and the detection of shallow bias in paleomagnetic inclinations: Was the ancient magnetic field dipolar? Timescales of the Paleomagnetic field. *American Geophysical Union, Geophysical Monograph Series*, *145*, 101–115. https://doi.org/10.1029/145GM08

Tauxe, L., Kent, D. V., & Opdyke, N. D. (1980). Magnetic components contributing to the NRM of Middle Siwalik red beds. *Earth and Planetary Science Letters*, *47*(2), 279–284. https://doi.org/10.1016/0012-821X(80)90044-8

Tauxe, L., Mullender, T., & Pick, T. (1996). Potbellies, wasp-waists, and superparamagnetism in magnetic hysteresis. *Journal of Geophysical Research*, *101*(B1), 571–583. https://doi.org/10.1029/95JB03041

Till, J., Guyodo, Y., Lagroix, F., Morin, G., & Ona-Nguema, G. (2015). Goethite as a potential source of magnetic nanoparticles in sediments. *Geology*, *43*, 75–78. https://doi.org/10.1130/G36186.1

Tong, Y., Yang, Z., Mao, C., Pei, J., Pu, Z., & Xu, Y. (2017). Paleomagnetism of Eocene red-beds in the eastern part of the Qiangtang Terrane and its implications for uplift and southward crustal extrusion in the southeastern edge of the Tibetan Plateau. *Earth and Planetary Science Letters*, *475*, 1–14. https://doi.org/10.1016/j.epsl.2017.07.026

Tsuchiyama, Y., Zaman, H., Sotham, S., Samuth, Y., Sato, E., Ahn, H.-S., et al. (2016). Paleomagnetism of Late Jurassic to Early Cretaceous red beds from the Cardamom Mountains, southwestern Cambodia: Tectonic deformation of the Indochina Peninsula. *Earth and Planetary Science Letters*, *434*, 274–288. https://doi.org/10.1016/j.epsl.2015.11.045

van der Voo, R., & Torsvik, T. H. (2012). The history of remagnetization of sedimentary rocks: Deceptions, developments and discoveries. *Geological Society, London, Special Publications*, *371*(1), 23–53.

Weibel, R., & Grobety, B. (1999). Pseudomorphous transformation of goethite needles into hematite in sediments of the Triassic Skagerrak Formation, Denmark. *Clay Minerals*, *34*(4), 657–660. https://doi.org/10.1180/000985599546415

Xian, H., Zhang, S., Li, H., Xiao, Q., Chang, L., Yang, T., & Wu, H. (2019). How did South China connect to and separate from Gondwana? New paleomagnetic constraints from the middle Devonian red beds in South China. *Geophysical Research Letters*, *46*, 7371–7378. https://doi.org/10.1029/2019GL083123

Yamashita, I., Surinkum, A., Wada, Y., Fujihara, M., Yokoyama, M., Zaman, H., & Otofuji, Y.-i. (2011). Paleomagnetism of the Middle–Late Jurassic to Cretaceous red beds from the Peninsular Thailand: Implications for collision tectonics. *Journal of Asian Earth Sciences*, *40*(3), 784–796. https://doi.org/10.1016/j.jseaes.2010.11.001

Zhang, Y., Huang, W., Huang, B., van Hinsbergen, D. J. J., Yang, T., Dupont-Nivet, G., & Guo, Z. (2018). 53–43 Ma deformation of the Eastern Tibet revealed by three stages of tectonic rotation in the Gongjue basin. *Journal of Geophysical Research: Solid Earth*, *123*, 3320–3338. https://doi.org/10.1002/2018JB015443

Zhang, Y., Huang, W., Zhang, Y., Poujol, M., Guillot, S., Roperch, P., et al. (2019). Detrital zircon provenance comparison between the Paleocene-Eocene Nangqian-Xialaxiu and Gongjue basins: New insights for Cenozoic paleogeographic evolution of the eastern Tibetan Plateau. *Palaeogeography, Palaeoclimatology, Palaeoecology*, *533*, 109241.